CVD Growth of Single-Walled Carbon Nanotubes with Narrow Diameter Distribution over Fe/MgO Catalyst and Their Fluorescence Spectroscopy

Hiroki Ago,*,† Shingo Imamura,† Toshiya Okazaki,‡ Takeshi Saito,‡ Motoo Yumura,‡ and Masaharu Tsuji†

Institute for Materials Chemistry and Engineering, Kyushu University, Kasuga 816-8580, Kyushu, Japan, and CREST, Japan Science and Technology, Restearch Center for Advanced Carbon Materials, National Institute for Advanced Industrial Science and Technology (AIST), Tsukuba 305-8565, Japan

Received: January 18, 2005; In Final Form: April 6, 2005

Single-walled carbon nanotubes (SWNTs) with a narrow diameter distribution are synthesized by thermal chemical vapor deposition (CVD) of methane over Fe/MgO catalyst on the basis of parametric study considering Fe loading, reaction temperature and time, methane concentration, and structure of a support material. We found that the porous MgO support gives the SWNTs with a narrow diameter distribution with the mean diameter and standard deviation of 0.93 and 0.06 nm, respectively, only when the Fe loading and reaction temperature are relatively low. The higher Fe loading and/or the higher reaction temperature enlarged the nanotube diameter, forming double-walled carbon nanotubes (DWNTs) in addition to SWNTs. This result indicates that only the diameter of Fe nanoparticles determines the growth of either SWNTs or DWNTs on the MgO support. The fluorescence and absorption spectra of the nanotube dispersion in D_2O solution with sodium dodecyl sulfate (SDS) were studied to identify their chirality distribution. The fluorescence of the uniform-diameter SWNTs indicates the formation of the near armchair structures. On the other hand, the SWNTs synthesized over the catalyst with a high Fe loading, 3 wt %, showed a wide chirality distribution including the near zigzag structure. The synthesis of the SWNTs with a narrow diameter distribution could be applied to the selection of SWNTs with a specific chirality based on postsynthesis separation.

Introduction

Single-walled carbon nanotubes (SWNTs) show unique physical properties originating in their one-dimensional structure with a nanoscale diameter and highly π-conjugated network. The chirality-dependent electronic structure, mechanical flexibility, high surface area, and high aspect ratio promise applications in the field of nanotechnology, such as nanodevices, nanosensors, and tips for probe microscopes.[1] It is essential for theses applications to control the structural geometry of nanotubes, i.e., diameter, length, number of walls, and chirality, which determine the electronic structure of a nanotube. In particular, the precise control of the chirality is still a big challenge but necessary for the future nanoelectronics and optoelectronics applications. For this purpose, the control over the SWNT diameter should be addressed in advance. The uniform diameter nanotubes are also important for encapsulation of molecules, like peapods (C_{60}-encapsulated SWNT).

Chemical vapor deposition (CVD), thermal pyrolysis of hydrocarbon, CO, or alcohol over transition metal nanoparticles, has been emerging as a powerful method for the synthesis of SWNTs. This is because CVD is capable of producing a large number of SWNTs[2−6] and a patterned network of SWNTs on a substrate for the device fabrication.[7,8] The diameter and yield of SWNTs are closely related to the size and composition of metal particle catalysts. As the metal particles have high surface energy, the particles tend to coalesce at high reaction temperatures used for CVD (typically 700−900 °C). To prevent the particles from coalescing, the inorganic porous materials, such as alumina (Al_2O_3),[9−11] silica (SiO_2),[12,13] magnesia (MgO),[14−18] zeolite,[19,20] and mesoporous silica,[21−23] are used to stabilize the fine metal particles. The porous support can produce a number of metal particles due to their high surface area, which is also advantageous to the high yield synthesis of SWNTs.

Because of the inhomogeneous surface structure of porous supports, the metal catalyst particles tend to have a broad size distribution. Therefore, the SWNTs synthesized by CVD generally have a broader diameter distribution compared with those synthesized by a laser-ablation method.[9,10] However, the recent progress of the CVD synthesis of SWNTs over porous materials can produce relatively uniform diameter SWNTs through the control of the catalyst metal size.[12,14,15,22] For the control of the nanotube diameter and chirality, it is of great importance to understand the formation process of the metal nanoparticles as well as a required condition, but they are not fully understood yet.

The recent breakthrough of dispersing isolated SWNTs in D_2O and the photoluminescence measurement offered a new technique to determine the chirality distribution of semiconducting SWNTs.[24,25] It was reported that the narrow diameter SWNTs tend to have a small number of chiral vector indices compared with those synthesized by a high-pressure CO disproportionation (HiPco) process. Bachilo and Miyauchi reported the predominance existence of (6,5) and (7,5) chiralities for the SWNTs synthesized by CoMoCAT process and alcohol CVD, respectively.[13,19]

Recently, we have studied that the growth of SWNTs and double-walled carbon nanotubes (DWNTs) over size-controlled Fe particles supported on MgO in terms of the metal−support interaction.[26,27] The MgO support offered a high nanotube yield

* To whom correspondence should be addressed. E-mail: ago@cm.kyushu-u.ac.jp.
† Kyushu University and CREST-JST.
‡ AIST.

10.1021/jp050307q CCC: $30.25
Published on Web 05/04/2005

due to the strong metal−support interaction. The MgO support has another advantage that it can be removed by the relatively mild acidic treatment,[16] while many support materials, such as alumina, silica, and zeolite, require the highly toxic HF treatment.

Here, we report the growth of SWNTs with a narrow diameter distribution over Fe particles supported on porous MgO. These SWNTs can be obtained only under specific conditions: a relatively low metal concentration (0.6 wt %) and low reaction temperature (750 °C). Increase in the Fe loading and/or reaction temperature broadens the SWNT diameter distribution and catalyzes the DWNT growth at the same time. The fluorescence spectra are studied for the dispersion of nanotubes to investigate the diameter and chirality distributions.

Experimental Section

Materials. The catalyst was prepared by mixing iron nitrate nonahydrate ($Fe(NO_3)_3 \cdot 9H_2O$; Wako Pure Chemical Industries, 99.9%) with MgO powder, using sonication in methanol for 1 h, followed by evaporation at 65 °C and 337 hPa. The dried powder was slightly pulverized and used as the catalyst for CVD without calcination. Two types of MgO powder, porous MgO (Wako) and crystalline MgO (Kishida Chemical), were used as the support material. The weight ratio of Fe to MgO was varied from 0.01 to 3 wt %.

Reaction. For the growth of carbon nanotubes, the catalyst (ca. 100 mg) was set in a quartz tube of 30 mm diameter and heated to the reaction temperatures, 700−850 °C, with a constant heating rate of 13 °C /min under an Ar flow (150 cm^3/min). At the reaction temperature, the Ar gas was switched to a mixture of CH_4 (20 vol %) and Ar with a total flow rate of 700 cm^3/min at atmospheric pressure. The reaction lasted for 10 min, unless otherwise stated. After the reaction, the system was cooled under an Ar flow.

Characterization. The samples were characterized by using a transmission electron microscope (TEM, JEOL 2100F) with an accelerating voltage of 200 kV. For TEM measurements, a sample was directly pressed onto a TEM grid to avoid effects of the solvent and sonication. X-ray diffraction (XRD) profiles were measured with RIGAKU RINT2100HLR and MultiFlex. The carbon products were characterized by Raman spectroscopy (JASCO NRS-2000) with the excitation wavelength of 514.5 nm and a laser spot size of ca. 0.1 mm. The spectra taken at three different places are averaged to minimize dispersion of the sample position.

For the optical measurements, the as-prepared nanotubes were treated by following the method reported by O'Connell et al.[24] The as-prepared nanotubes were dispersed in D_2O with 1 wt % of sodium dodecyl sulfate (SDS) and sonicated by using a horn-type homogenizer (SONICS vibracell VCX-500) with 50 W power for 10 min. The nanotube dispersion was ultracentrifuged with the force of 125,600 G for 150 min, using a HITACHI CP100MX with a vertical-type rotator (P56ST). The supernatant was collected and subjected to the absorption and fluorescence measurements. The absorption was measured with a SHIMADZU UV-3150 spectrometer. The fluorescence spectra were taken with a J−Y Fluorolog-3 spectrometer equipped with an electrically cooled InP/InGaAs detector (HAMAMATSU HP-9170-75). The scan steps were set 5 nm on both excitation and emission axes. Both the incident beam and photodetector were calibrated before the measurement.

Results and Discussion

Metal Concentration Dependence. In Figure 1a, we show the TEM image of the as-received porous MgO powder. It consists of small pieces of MgO fragments that form nanoscale void spaces. The surface area of the porous MgO powder is 149 m^2/g, as measured by N_2 adsorption. The XRD profile (Figure 1b) showed broad diffraction peaks, indicating the small crystalline size of the MgO fragments. The crystalline size was calculated to be 10.9 nm from a Scherrer's equation. This porous MgO powder was mixed with iron nitrate in methanol and dried in a vacuum to use as the catalyst for the CVD growth of carbon nanotubes. During elevation of the temperature for the CVD, the supported iron nitrate decomposed to form fine Fe particles which act as the seeds of the SWNT or DWNT growth. Parts c and d of Figure 1 show the TEM image and the corresponding XRD profile of the crystalline MgO powder, which will be discussed later.

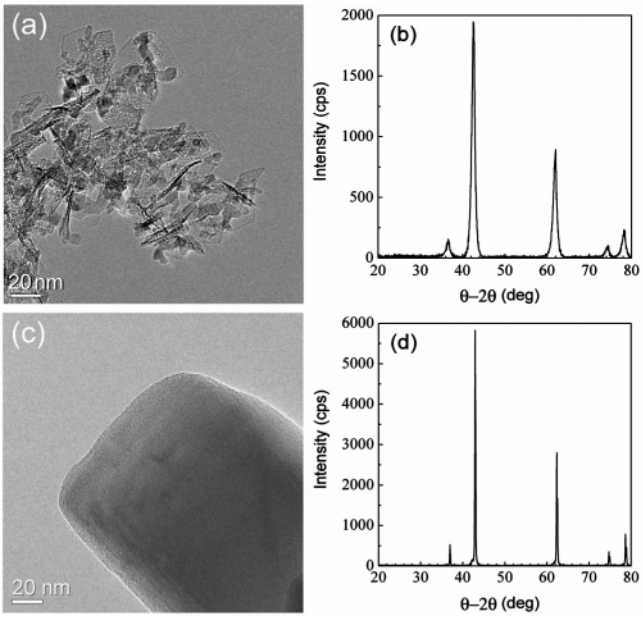

Figure 1. TEM images and XRD profiles of as-received MgO: (a,b) porous MgO and (c,d) crystalline MgO powder.

Carbon nanotubes were obtained by the CVD of methane at 750 °C for 10 min. Figure 2 shows the TEM image of the carbon product obtained on the Fe/porous MgO catalysts with two different Fe loadings, [Fe]/[MgO] = 0.6 and 3 wt %. We found that the low Fe concentration gives only SWNTs with almost no DWNTs and MWNTs. The histogram of the SWNT diameter is displayed in Figure 2e. It shows that the SWNTs have small diameters with a narrow distribution; the mean diameter and standard derivation are 0.93 and 0.06 nm, respectively. Due to the porous structure of the MgO support, the roots of SWNTs were hardly observed. When we increased the Fe loading to 3 wt %, DWNTs were frequently observed together with SWNTs, as shown in Figure 2d. Note that more than 20% of nanotubes are DWNTs. The increase of the SWNT diameter and the broadened diameter distribution were also observed; the mean diameter and standard deviation are 1.35 and 0.45 nm, respectively (Figure 2f). It has been reported that DWNTs can be grown selectively over various support material,[11,17,20,26,] but this is the first demonstration that the relative abundance of SWNTs to DWNTs is sensitive to the metal concentration. Our result indicates the importance of the particle size of the metal catalyst to determine the growth of either SWNTs or DWNTs.

The Raman spectra measured at three different Fe loadings, 0.6, 1.5, and 3 wt %, are shown in Figure 3. The spectra of carbon nanotubes are characterized by four main signals, G-band, D-band, Breit−Wigner−Fano (BWF) line, and radial

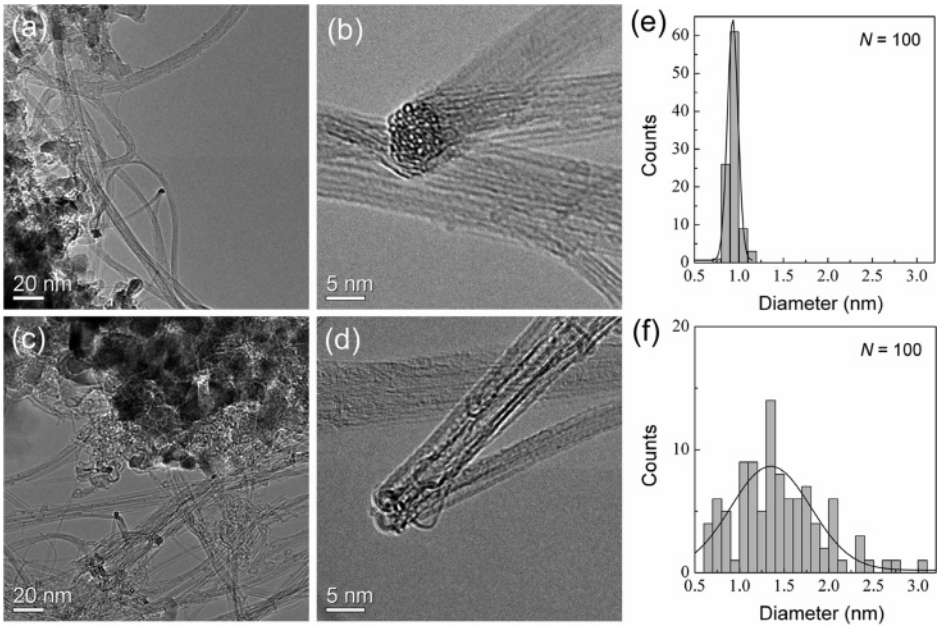

Figure 2. TEM images of carbon nanotubes grown over (a, b) Fe 0.6 wt % and (c, d) 3 wt % supported on the porous MgO. The nanotube growth was performed at 750 °C for 10 min under a 20 vol % of CH_4 flow diluted with Ar. The histograms of the outer diameter of nanotubes determined from TEM images are plotted in (e) 0.6 wt % and (f) 3 wt %. At 0.6 wt %, only SWNTs were observed, while 3 wt % loading gave 26 DWNTs and 74 SWNTs out of 100 nanotubes. The solid lines correspond to Gaussian fits.

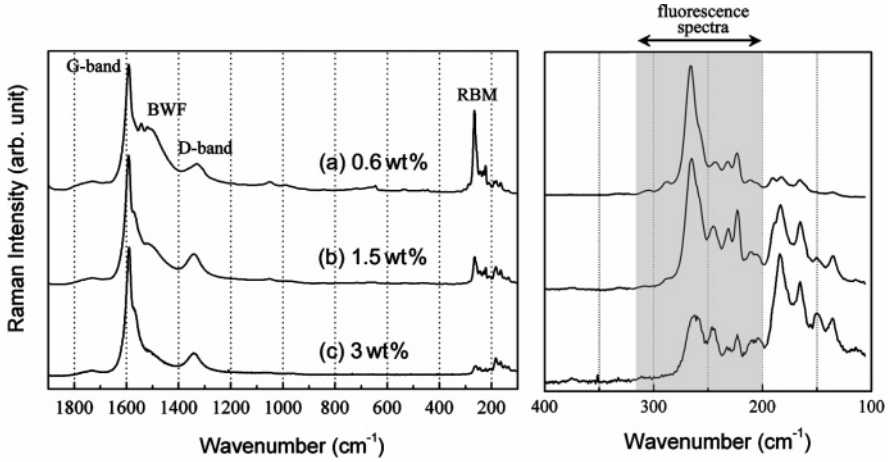

Figure 3. Raman spectra of carbon nanotubes grown over the Fe/porous MgO catalysts with three different Fe loadings: (a) 0.6, (b) 1.5, and (c) 3 wt %. The reaction condition is 750 °C for 10 min with 20 vol % of CH_4 in Ar. The spectra in the left panel are normalized to the G-band at ca. 1591 cm^{-1}. The right panel shows the magnified spectra corresponding to the RBM signals, in which the RBM signals are normalized to the strongest peak. The excitation wavelength and spot size are 514.5 nm and 0.1 mm, respectively. Spectra taken for three different positions are averaged to minimize the dispersion of the sample position. The grayed area shows the region where the fluorescence can be detected in our system (see Figure 7).

breathing mode (RBM),[28] as indicated in Figure 3a. The G-band that appears at around 1591 cm^{-1} is ascribed to tangential modes of the graphene sheet. The D-band at around 1338 cm^{-1} is related to the defects in the graphene sheet and to the presence of amorphous carbon. The BWF line at around 1500 cm^{-1} is a characteristic Raman mode of metallic nanotubes. The RBM peaks for the lower frequency modes below 500 cm^{-1} originate in nanotubes with diameters less than 3 nm, and their peak position is dependent on the nanotube diameter with the following equation[29]

$$\omega_r = 232/d + 6.5 \qquad (1)$$

where ω_r (cm^{-1}) and d (nm) are the Raman shift of the RBM peaks and the nanotube diameter, respectively.

From Figure 3, one can see that the RBM peak intensities are very sensitive to the Fe loading. At the low Fe loading of 0.6 wt %, a strong RBM peak was observed at 265 cm^{-1}, which corresponds to nanotubes with 0.90 nm diameter. Much weaker sidebands are also present in the spectrum, covering the diameters of 1.0−1.5 nm. Taking into account the histogram of the diameter based on TEM observations shown in Figure 2e, this represents the growth of the SWNTs with a narrow diameter distribution. However, we should also consider the peak intensity of the RBM peaks does not represent the real abundance. This is because the Raman scattering of SWNTs occurs through a resonant process associated with optical transition with the excitation laser light.[12,28,29] According to a Kataura plot,[30] the SWNTs resonanced with a 514.5 nm laser light are supposed be metallic nanotubes, as is understood by the presence of the strong BWF line at around 1500 cm^{-1}. The possible chiral index for the metallic SWNTs is (8,5) with the diameter of 0.902 nm from the work by Strano et al.[31] At the

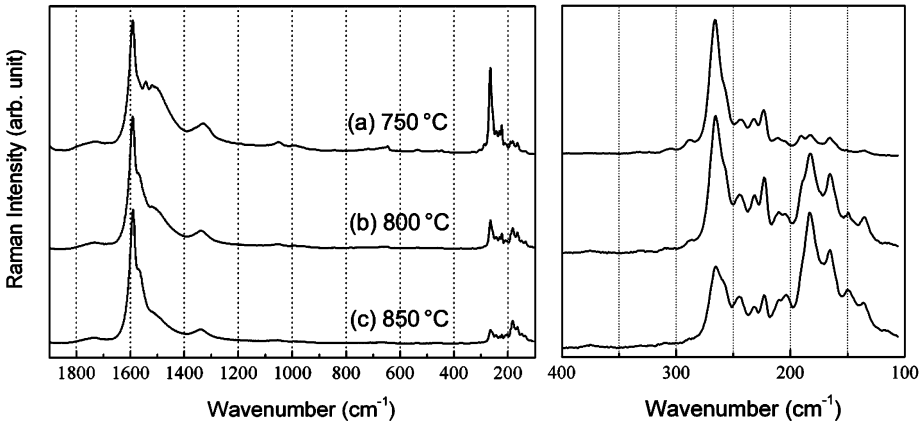

Figure 4. Reaction temperature dependence of the Raman spectra of nanotubes grown over the Fe 0.6 wt % supported on porous MgO catalysts: (a) 750, (b) 800, and (c) 850 °C.

present excitation wavelength, the semiconducting nanotubes with 1.3−1.7 nm should show resonance with the present excitation wavelength.[29] However, since the relative peak intensity of the RBM signals below 200 cm^{-1} corresponding to these thick semiconducting nanotubes is much weaker than the main signal at 265 cm^{-1}, we can conclude that the as-prepared SWNTs have narrow and uniform diameters around 0.90 nm.

The D-band signal originating in structural defects in SWNTs and/or amorphous carbons was clearly observed together with a strong G-band in Figure 3a, indicating imperfect graphitic structure due to the low reaction temperature of 750 °C. We note that the Raman spectrum with the lower Fe concentration of less than 0.5 wt % was very weak, suggesting the Fe concentration is not high enough to form fine Fe particles on the porous MgO.

When we increased the Fe loading to 1.5 and 3 wt %, the RBM peaks at the lower wavenumbers became stronger (Figure 3b,c). In particular, the peak at 182 cm^{-1} corresponding to the 1.32 nm diameter nanotubes increased with an increase in the Fe loading. Note that the change in the Raman spectrum is in good agreement with the formation of DWNTs and thick SWNTs (see Figure 2f).[26] Accompanying the decrease of the 260 cm^{-1} peak, which corresponds to the metallic SWNTs, the BWF line at 1500 cm^{-1} decreased. The D-band was found not to be so sensitive to the Fe concentration. This is quite reasonable considering the relatively low reaction temperature (750 °C).

Reaction Conditions. Figure 4 shows the temperature dependence of the Raman spectrum for the nanotubes grown over Fe 0.6 wt %/porous MgO catalyst. The temperature as well as the Fe concentration were found to strongly affect the nanotube diameter distribution from the change of the RBM peak intensities; the higher temperature gives the thicker nanotubes with a broader diameter distribution (see Figure 3). As is expected, the nanotubes obtained at 850 °C contained DWNTs. In our previous TEM study, the nanotube diameter (either SWNTs or DWNTs) is found to be closely related to that of the Fe particle located at the root of the nanotube.[27] Hence, the observed broadening in the nanotube diameter is understood by the increase in the diameter of Fe particles. Therefore, the increase in the nanotube diameter at the higher reaction temperature can be interpreted as the acceleration of thermal sintering of the metal nanoparticles.[12,19] One major difference from the effects of Fe loading is the reduction of the D-band intensity with the increase of the reaction temperature, suggesting the crystallinity of nanotubes is dependent on the reaction temperature. This fact indicates that the higher temperature is preferable for the growth of high-quality SWNTs and DWNTs when methane is used as a carbon source.

Not only the reaction temperature, but also the reaction time was found to influence the Raman spectra of nanotubes. We studied the Raman spectrum as a function of the reaction time, 10, 30, and 120 min, at 750 °C. The result is shown in the Supporting Information. It was found that the longer reaction time resulted in the wide SWNT diameter distribution. Therefore, the thermal sintering of Fe particles is supposed to proceed slowly even at 750 °C. We also studied effects of CH_4 concentration, 10, 20, and 100 vol %, during the CVD at 750 °C for 10 min. The carbon yield increased with increasing the CH_4 concentration, but the Raman spectra looked similar for all the concentrations (not shown). This suggests that the Fe particle size is not so sensitive to the CH_4 concentration, unlike the reaction temperature and time.

In our previous papers, we reported the growth of DWNTs and SWNTs over the colloidal Fe particles with two different diameters, 4 and 10 nm, supported on MgO.[26,27] The diameter of Fe particles was reduced to 0.5−3.5 nm, which is suitable for the nanotube growth, when they are annealed on the MgO support.[26] The observed size reduction was accounted for by the strong metal−support interaction.[27] In that case, the diameters of DWNTs and SWNTs were large and had a broad distribution. The Fe particles with an initial diameter of 4 nm resulted in the DWNTs with the outer diameters of 1.2−2.8 nm (1.7 nm mean diameter), while the 10 nm particles gave DWNTs with 1.2−4 nm diameter (2.2 nm mean diameter).[26] Our present result shows that the thermal decomposition of iron nitrate over the porous MgO gives smaller and more uniform metal particles than those formed by size reduction of the Fe particles with 4 and 10 nm diameters. Note that the Fe nanoparticles with small and uniform diameters can be realized only at a specific condition; the low Fe loading and low reaction temperature, and short reaction time. Therefore, we think that the diameters of 1.5−3 nm are the most stable size for the Fe particles on MgO under the normal CVD condition.[26] Because (i) the particle is slightly larger for SWNT growth and (ii) MgO itself can decompose methane gas to provide carbon atoms to Fe particles, the growth of DWNTs has been frequently observed for MgO supports.[16−18]

Effects of Support Material. Porous materials are widely used to support metal particles in the CVD growth of nanotubes. Here, we study effects of the nanoporous structure by comparing the crystalline MgO (see the TEM image in Figure 1c) with the porous MgO (Figure 1a). The crystalline MgO contains few

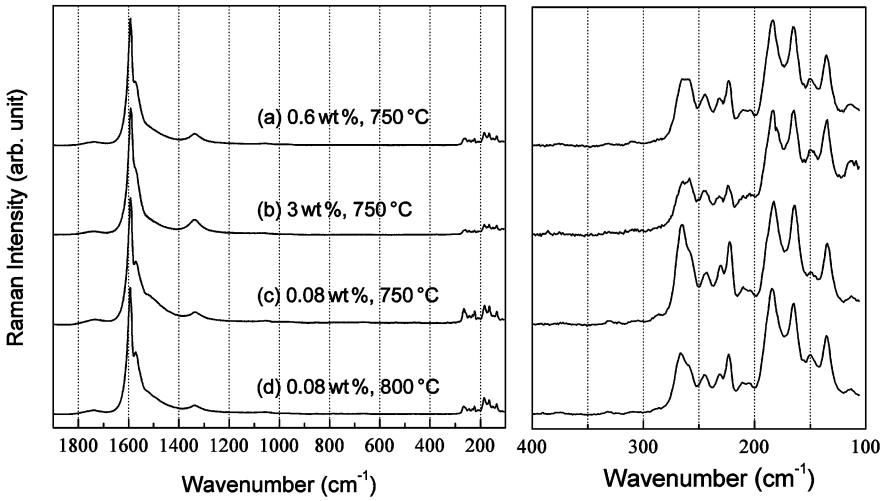

Figure 5. Raman spectra of carbon nanotubes formed over the crystalline MgO support for different Fe loading and reaction temperature: (a) 0.6 wt %, 750 °C; (b) 3 wt %, 750 °C; (c) 0.08 wt %, 750 °C; and (d) 0.08 wt %, 800 °C.

nanopores, and the corresponding XRD profile shown in Figure 1d has narrower peak widths compared with those of the porous MgO (Figure 1b). The crystalline size estimated from the XRD line width is 107 nm, which is about 10 times larger than that of the porous MgO (10.9 nm). The surface areas measured by the N_2 adsorption of porous and crystalline MgO were 149 and 14 m^2/g, respectively. So, there is a significant difference in the nanoscale morphology in these MgO support materials. The Fe-supported crystalline MgO powder was prepared by the same procedure as that used for the porous MgO for the CVD growth of nanotubes.

The nanotubes grown over the Fe/crystalline MgO were analyzed by Raman spectroscopy, as indicated in Figure 5. In contrast to the catalyst using the porous MgO, the catalyst using the crystalline MgO resulted in a broad distribution in the nanotube diameter, irrespective of the Fe loading and reaction temperature. The Raman spectrum of the nanotubes synthesized at 750 °C with 0.6 wt % of Fe loading (Figure 5a) is quite different from that grown on porous MgO under the same conditions (Figure 3a). Almost no change was seen for the higher Fe loading of 3 wt % (Figure 5b). This is probably explained by the low surface area of the crystalline MgO support (14 m^2/g). Because of the low surface area, the Fe loading of 0.6 wt % could still too high to grow thin SWNTs.

Therefore, we tried to grow thin SWNTs over the crystalline MgO catalyst by lowering the Fe loading. As illustrated in Figure 5c, the low Fe loading of 0.08% resulted in the increase in the relative intensity of the RBM signal to the G-band together with the increase of the RBM peak at 265 cm^{-1} (corresponding to the 0.90 nm diameter nanotubes). This effect was also observed at 800 °C, although it was weakened slightly (Figure 5d). In addition, the D-band was found to be suppressed for the 0.08 wt % loading, suggesting that the low metal concentration is preferable for the crystalline MgO. However, the nanotube diameter is not so uniform when compared with the SWNTs grown over Fe 0.6 wt % supported on the porous MgO. Further reduction of the Fe loading did not give the nanotubes. Therefore, we can conclude that the porous network in the support material plays an essential role in the growth of small diameter SWNTs. We speculate that the porous network, in other words, the walls of nanopores, stabilizes the fine metal particles with a diameter around 0.9 nm due to the strong metal−support interaction.[23]

Absorption Spectra. The optical properties, absorption and fluorescence, were studied to characterize the diameter and chirality distributions for the nanotubes grown over Fe/porous MgO catalysts. The nanotube dispersion in D_2O containing 1 wt % of the anionic surfactant, SDS, was subjected to the sonication and ultracentrifuge to obtain isolated nanotubes leaving sediments of the catalyst and nanotube bundles. Bundles of SWNTs are sedimented during the ultracentrifuge, because the bundles have a higher weight density than D_2O.[24] We found that the dispersion of the SWNTs grown over Fe 0.6 wt %/porous MgO is a dark black solution, while the dispersion of the nanotubes grown over Fe 3 wt % on porous MgO, which are the mixture of SWNTs and DWNTs, is much more transparent.

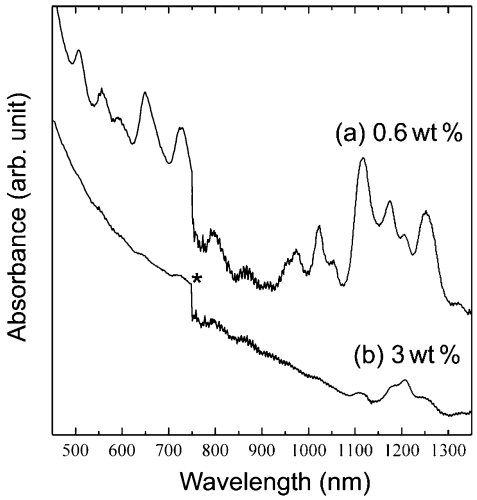

Figure 6. Optical absorption spectra of carbon nanotubes grown over (a) Fe 0.6 wt % and (b) Fe 3 wt % supported on the porous MgO at 750 °C for 10 min. The nanotubes were dispersed in D_2O solution containing 1 wt % of SDS, followed by sonication and ultracentrifuge. An asterisk (*) identifies the step due to the change of the photodetectors.

In Figure 6, the UV−vis−NIR spectra of low (0.6 wt %) and high (3 wt %) Fe loadings are shown. The dispersion prepared from the carbon product with the low Fe loading, which contains only SWNTs, shows a number of sharp absorption bands. This is attributed to the absorption of the isolated SWNTs.[24] On the other hand, thick SWNTs and DWNTs grown under the high Fe loading condition (Figure 6b) showed the poorly resolved spectrum with weak absorbance, which is consistent with the observed transparency of the nanotube dispersion. We speculate that isolated DWNTs have a higher

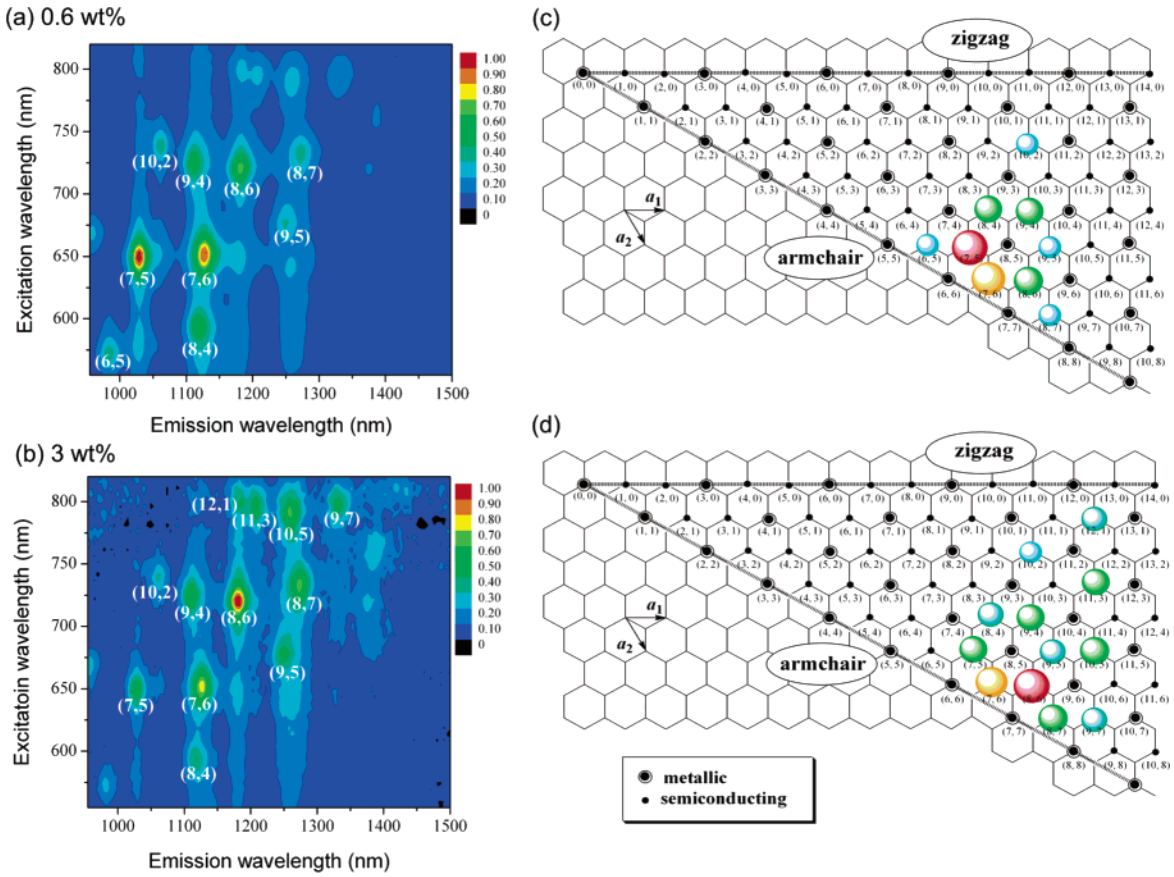

Figure 7. Contour plots of fluorescence spectra of excitation and emission wavelengths for the different Fe loadings, (a) 0.6 and (b) 3 wt %. The nanotube dispersions used for this fluorescence measurement are the same as those used for the optical absorption measurement in Figure 6. The Raman spectra of the samples in parts a and b are shown in Figure 3a and Figure 3c, respectively. In the right panel of Figure 3, the region where the fluorescence can be observed in our system is highlighted in gray. Fluorescence intensity and chirality distribution of the nanotubes are shown in the chiral vector maps c and d, determined from plots a and b, respectively. The area of the circle shows the peak intensity, and the color corresponds to that of the contour plot. The chiral vector map is referred from ref 28.

weight density than SWNTs so that DWNTs are sedimented during the ultracentrifuge process. In addition, the present surfactant, SDS, may not be suitable for dispersing DWNTs with relatively large diameters, as is reported by Lebedkin et al.[32]

Fluoresence Spectra. Recently, it has been shown that the chiralities of semiconducting nanotubes can be determined from the correlation of excitation and emission energies of the fluorescence spectrum.[25] The contour maps of the fluorescence spectra are plotted in Figure 7a,b, where the peak intensities are normalized to the strongest emission peak. The dispersed solutions were identical with those used for the absorption measurement (Figure 6). The contour maps showed clear peaks which can be assigned to the nanotubes with specific chiral vectors.[25] Chiral indices obtained from the fluorescence spectra are illustrated in Figure 7c,d. The chirality distribution is found to strongly depend on the Fe loading; the low (or high) Fe loading gives the small (large) tube diameters with a relatively narrow (wide) chirality distribution. Note that the metallic SWNT with (8,5) chiral vector with $d = 0.902$ nm estimated from the Raman spectrum for the Fe 0.6 wt %[31] falls into the appropriate position in the chiral map shown in Figure 7c. One can see some tendency that the narrow SWNTs (Fe 0.6 wt %; Figure 7c) have strong peak intensities corresponding to the nanotubes with near armchair structures, while thick nanotubes (Fe 3 wt %; Figure 7d) have a wide chirality distribution including the near zigzag structure. This is also pointed out for the SWNTs synthesized by alcohol CVD over the Fe−Co/zeolite catalyst.[19] Bachilio and Miyauchi found the predominant signals at (6,5) and (7,5) nanotubes,[13,19] but the peak intensity is not so dominant in our samples, probably because their samples are thinner than ours. It is also noted that Lebedkin et al. reported the PL spectra indicating near armchair-rich structures for the SWNTs grown by the laser-ablation.[33] Our fluorescence contour map is consistent with these previous reports using SDS as the surfactant.

The nanotubes formed under the high Fe loading, 3 wt %, showed a poorly solved absorption spectrum (Figure 6b), which suggests the imperfect dispersion, low concentration of nanotubes, or presence of large diameter nanotubes. Actually, the observed fluorescent intensity was weaker than that of the low Fe loading, 0.6 wt %. The fluorescence spectra of nanotubes grown over the 3 wt %/porous MgO indicates the presence of thicker nanotubes compared with SWNTs grown over the 0.6 wt %/MgO catalyst, which is consistent with the observed Raman spectrum shown in Figure 3c. Due to the limitations of the fluorescence measurement, nanotubes with a diameter larger than 1.3 nm cannot be detected in our system, and the region where we can measure the fluorescence in our system is highlighted in the right panel of Figure 3. It is unclear whether the observed luminescence occurs from SWNT or the inner wall of DWNTs in the present dispersion, but it is likely a small number of isolated SWNTs emit fluorescence due to the higher weight density of DWNTs. Because a DWNT should have a higher weight density than a SWNT due to two concentric graphene shells, isolate DWNTs tend to sediment during the ultracentrifuge with isolated SWNTs remaining in the supernatant. At the moment, it is difficult to discuss the absolute

concentration or relative abundance of nanotubes with a specific chirality, because the fluorescence efficiency of individual SWNT with each chirality is unknown. Further study is necessary to understand the physics behind the observed fluorescence.

Our study revealed that with the appropriate selection of catalyst and the CVD conditions, we are able to control the nanotube diameter. The control over the nanotube diameter means that we can control the chirality distribution of nanotubes to a certain extent. Recently, separation of metallic and semiconducting SWNTs on the basis of specific interaction or different electronic properties has been realized. The difference in the dielectric constants of metallic and semiconducting SWNTs was used to selectively deposit metallic SWNTs onto the electrodes.[34] The molecular interaction between SWNTs and adsorbed molecules or DNA has been applied for the diameter and/or chirality separation of SWNTs.[35] Therefore, the combination of the present synthesis of the uniform diameter SWNTs and new separation techniques may enable us to choose the specific SWNTs with one desired chiral index.

Conclusions

The CVD growth of SWNTs and DWNTs over Fe-supported MgO catalysts is studied in terms of the control of their diameter distribution by considering the Fe loading, reaction temperature and time, methane concentration, and structures of the MgO support. The SWNTs with a narrow diameter distribution, 0.93 $\pm$ 0.06 nm determined from the TEM analysis, can be synthesized only when the both Fe loading and reaction temperature are low and the reaction time is short. This diameter is similar to that observed by the Raman spectrum (0.90 nm). This narrow diameter distribution was observed for the porous MgO powder, but not for the crystalline MgO powder. These results indicate that the formation of fine nanoparticles with a diameter of around 1 nm is realized only at the specific condition with the aid of walls of nanopores existing in the support. We also found that the high Fe loading and/or high reaction temperature resulted in the growth of DWNTs together with thick SWNTs, resulting in an inhomogeneous diameter distribution.

The fluorescence spectra of D_2O dispersions of as-prepared nanotubes were used to identify the diameter and chirality distribution. The SWNTs with a narrow diameter distribution showed a relatively narrow chirality distribution with the near armchair-rich structures. The nanotubes with a broad diameter distribution tended to sediment during the ultracentrifuge and showed the broad chirality distribution including near zigzag structure. We believe that the combination of the present finding of the SWNT synthesis and the new separation techniques[34,35] enables us to choose the specific SWNTs with one desired chiral index, which is essential for future SWNT-based nanoelectronics and optoelectronics applications.

Acknowledgment. The authors acknowledge Dr. T. Setoguchi, Mr. N. Tomonaga, and Dr. A. Tanaka of Mitsubishi Heavy Industries for helpful discussions, and are grateful to Prof. I. Mochida and Prof. Y. Korai of Kyushu University for the use of the Raman and the TEM (JEOL 2100F). H.A. acknowledges the help of the Center of Advanced Instrumental Analysis for the XRD measurements. This work was supported by KAKENHI (No. 16710087), CREST Program of JST, Nano-Carbon Technology Project of NEDO, and Nissan Science Foundation.

Supporting Information Available: Raman spectra of nanotubes grown at 750 °C for 10 min with the different reaction times, 10, 30, and 120 min. This material is available free of charge via the Internet at http://pubs.acs.org.

References and Notes

(1) Baughman, R. H.; Zakhidov, A. A.; de Heer, W. A. *Science* **2002**, *297*, 787.
(2) Nikolaev, P.; Bronikowski, M. J.; Bradley, R. K.; Rohmund, F.; Colbert, D. T.; Smith, K. A.; Smalley, R. E. *Chem. Phys. Lett.* **1999**, *313*, 91.
(3) Cheng, H. M.; Li, F.; Su, G.; Pan, H. Y.; He, L. L.; Sun, X.; Dresselhaus, M. S. *Appl. Phys. Lett.* **1998**, *72*, 3282.
(4) Ago, H.; Ohshima, S.; Uchida, K.; Yumura, M. *J. Phys. Chem. B* **2001**, *105*, 10453. Saito, T.; Ohshima, S.; Xu, W. C.; Ago, H.; Yumura, M.; Iijima, S. *J. Phys. Chem. B*, in press.
(5) Su, M.; Zheng, B.; Liu, J. *Chem. Phys. Lett.* **2002**, *322*, 321.
(6) Hata, K.; Futaba, D. N.; Mizuno, K.; Namai, T.; Yumura, M.; Iijima, S. *Science* **2004**, *306*, 1362.
(7) Franklin, N. R.; Dai, H. *Adv. Mater.* **2000**, *12*, 890.
(8) Huang, S.; Maynor, B.; Cai, X.; Liu, J. *Adv. Mater.* **2003**, *15*, 1651.
(9) Dai, H.; Rinzler, A. G.; Nikolaev, P.; Thess, A.; Colbert, D. T.; Smalley, R. E. *Chem. Phys. Lett.* **1996**, *260*, 471.
(10) Peigney, A.; Coquay, P.; Flahaut, E.; Vandenberghe, R. E.; Grave, E. D.; Laurent, C. *J. Phys. Chem. B* **2001**, *105*, 9699.
(11) Liu, B. C.; Lyu, S. C.; Lee, T. J.; Choi, S. K.; Eum, S. J.; Yang, C. W.; Park, C. Y.; Lee, C. J. *Chem. Phys. Lett.* **2003**, *373*, 475.
(12) Alvarez, W. E.; Pompeo, F.; Herrera, J. E.; Balzano, L.; Resasco, D. E. *Chem. Mater.* **2002**, *14*, 1853.
(13) Bachilo, S. M.; Balzano, L.; Herrera, J. E.; Pompeo, F.; Resasco, D. E.; Weisman, R. B. *J. Am. Chem. Soc.* **2003**, *125*, 11186.
(14) Jeong, H. J.; An, K. H.; Lim, S. C.; Park, M. S.; Chang, J. S.; Park, S. E.; Eum, S. J.; Yang, C. W.; Park, C. Y.; Lee, Y. H. *Chem. Phys. Lett.* **2003**, *380*, 263.
(15) Li, Y.; Zhang, X.; Shen, L.; Luo, J.; Tao, X.; Liu, F.; Xu, G.; Wang, Y.; Geise, H. J.; Tendeloo, G. V. *Chem. Phys. Lett.* **2004**, *398*, 276.
(16) Flahaut, E.; Bacsa, R.; Peigney, A.; Laurent, C. *Chem. Commun.* **2003**, 1442.
(17) Li, W. Z.; Wen. J. G.; Sennett, M.; Ren, Z. F. *Chem. Phys. Lett.* **2003**, *368*, 299.
(18) Lyu, S. C.; Liu, B. C.; Lee, S. H.; Park, C. Y.; Kang, H. K.; Yang, C. W.; Lee, C. J. *J. Phys. Chem. B* **2004**, *108*, 2192.
(19) Miyauchi, Y.; Chiashi, S.; Murakami, Y.; Hayashida, Y.; Maruyama, S. *Chem. Phys. Lett.* **2004**, *387*, 198.
(20) Hiraoka, T.; Kawakubo, T.; Kimura, J.; Taniguchi, R.; Okamoto, A.; Okazaki, T.; Sugai, T.; Ozeki, Y.; Yoshikawa, M.; Shinohara, H. *Chem. Phys. Lett.* **2003**, *382*, 679.
(21) Zhu, J.; Yudasaka, M.; Iijima, S. *Chem. Phys. Lett.* **2003**, *380*, 496.
(22) Ciuparu, D.; Chen, Y.; Lim, S.; Haller, G. L.; Pfefferle, L. *J. Phys. Chem. B* **2004**, *108*, 503. Chen, Y.; Ciuparu, D.; Lim, S.; Yang, Y.; Haller, G. L.; Pfefferle, L. *J. Catal.* **2004**, *225*, 453.
(23) Ciuparu, D.; Chen, Y.; Lim, S.; Yang, Y.; Haller, G. L.; Pfefferle, L. *J. Phys. Chem. B* **2004**, *108*, 15565.
(24) O'Connell, M. J.; Bachilo, S. M.; Huffman, C. B.; Moore, V. C.; Strano, M. S.; Haroz, E. H.; Rialon, K. L.; Boul, P. J.; Noon, W. H.; Kittrell, C.; Ma, J.; Hauge, R. H.; Weisman, R. B.; Smalley, R. H. *Science* **2002**, *297*, 593.
(25) Bachilo, S. M.; Strano, M. S.; Kittrell, C.; Hauge, R. H.; Smalley, R. E.; Weisman, R. B. *Science* **2002**, *298*, 2361.
(26) Ago, H.; Nakamura, K.; Imamura, S.; Tsuji, M. *Chem. Phys. Lett.* **2004**, *391*, 308.
(27) Ago, H.; Nakamura, K.; Uehara, N.; Tsuji, M. *J. Phys. Chem. B* **2004**, *108*, 18908.
(28) Saito, R.; Dresselhaus, G.; Dresselhaus, M. S. *Physical Properties of Carbon Nanotubes*; Imperial College Press: London, UK, 1998.
(29) Alvarez, L.; Righi, A.; Guillard, T.; Rols, S.; Anglaret, E.; Laplaze, D.; Sauvajol, J. L. *Chem. Phys. Lett.* **2000**, *316*, 186.
(30) Kataura, H.; Kumazawa, Y.; Maniwa, Y.; Umezu, I.; Suzuki, S.; Ohtsuka, Y.; Achiba, Y. *Synth. Met.* **1999**, *103*, 2555.
(31) Strano, M. S.; Doorn, S. K.; Haroz, E. H.; Kittrell, C.; Hauge, R. H.; Smalley, R. E. *Nano Lett.* **2003**, *3*, 1091.
(32) Lebedkin, S.; Arnold, K.; Hennrich, F.; Krupke, R.; Renker, B.; Kappes, M. M. *New J. Phys.* **2003**, *5*, 140.1.
(33) Lebedkin, S.; Hennrich, F.; Skipa, T.; Kappes, M. M. *J. Phys. Chem. B* **2003**, *107*, 1949.
(34) Krupke, R.; Hennrich, F.; Lohneysen, H. v.; Kappes, M. M. *Science* **2003**, *301*, 344.
(35) Zheng, M.; Jagota, A.; Semke, E. D.; Diner, B. A.; Mclean, R. S.; Lustig, S. R.; Richardson, R. E.; Tassi, N. G. *Nat. Mater.* **2003**, *2*, 338.